

A novel *Plasmodium yoelii* pseudokinase, PypPK1, is involved in erythrocyte invasion and exflagellation center formation

Takahiro Ishizaki^{a,b}, Nattawat Chaiyawong^{a,b}, Hassan Hakimi^b, Masahito Asada^{a,b},
Mayumi Tachibana^c, Tomoko Ishino^c, Kazuhide Yahata^b, Osamu Kaneko^{a,b,*}

^a Program for Nurturing Global Leaders in Tropical and Emerging Communicable Diseases, Graduate School of Biomedical Sciences, Nagasaki University, 1-12-4 Sakamoto, Nagasaki 852-8523, Japan

^b Department of Protozoology, Institute of Tropical Medicine (NEKKEN), Nagasaki University, 1-12-4 Sakamoto, Nagasaki 852-8523, Japan

^c Division of Molecular Parasitology, Proteo-Science Center, Ehime University, Toon, Ehime 791-0295, Japan

ARTICLE INFO

Keywords:

Plasmodium yoelii
Pseudokinase
Exflagellation center
Sexual stage
Erythrocyte invasion
Malaria

ABSTRACT

Malaria parasites proliferate by repeated invasion of and multiplication within erythrocytes in the vertebrate host. Sexually committed intraerythrocytic parasites undergo sexual stage differentiation to become gametocytes. After ingestion by the mosquito, male and female gametocytes egress from erythrocytes and fertilize within the mosquito midgut. A complex signaling pathway likely responds to environmental events to trigger gametogenesis and regulate fertilization; however, such knowledge remains limited for malaria parasites. Several pseudokinases are highly transcribed at the gametocyte stage and are possible multi-functional regulators controlling critical steps of the life cycle. Here we characterized one pseudokinase, termed PypPK1, in *Plasmodium yoelii* that is highly expressed in schizonts and male gametocytes. Immunofluorescence assays for parasites expressing Myc-tagged PypPK1 confirmed that PypPK1 protein is expressed in schizonts and sexual stage parasites. Transgenic Δ pPK1 parasites, in which the PypPK1 gene locus was deleted by the CRISPR/Cas9 method, showed significant growth defect and reduced virulence in mice. In the blood stage, Δ pPK1 parasites were able to egress from erythrocytes similar to wild type parasites; however, erythrocyte invasion efficacy was significantly reduced. During sexual stage development, no clear changes were seen in male and female gametocytemias as well as gametocyte egress from erythrocytes; but, the number of exflagellation centers and oocysts were significantly reduced in Δ pPK1 parasites. Taken together, PypPK1 has an important role for both erythrocyte invasion and exflagellation center formation.

1. Introduction

Malaria remains a heavy burden on human society worldwide, causing > 200 million cases and > 400,000 deaths annually [1]. Malaria parasites proliferate by repeated invasion of and multiplication within erythrocytes in mammalian hosts. This asexual blood stage is responsible for malaria clinical symptoms and pathogenesis. During asexual proliferation, some parasites undergo sexual stage differentiation and matured gametocytes circulate in the host peripheral blood in anticipation of ingestion by a mosquito [2]. Although sexual stage parasites do not contribute to malaria pathogenesis, they are essential for transmission to other hosts by mosquito vectors. Therefore, sexual development in both mammalian hosts and vector mosquitoes has been

studied extensively to identify novel drug and vaccine targets to block parasite transmission [3].

Phosphorylation has a critical role to regulate various biological processes. Wide-scale proteomics and exhaustive phosphor-proteome analysis has revealed key roles of phosphorylation in both asexual and sexual stage malaria parasites [4–6]. In sexual stages, it has been shown to regulate gametogenesis, as well as exflagellation of male gametocytes [5,7]. Several calcium dependent protein kinases (CDPKs) play critical roles in gametogenesis. CDPK1-deleted parasites fail to egress from host erythrocytes and are not transmitted to mosquitoes [8]. CDPK2 has a role in exflagellation and CDPK4 plays a role in DNA replication during male gametogenesis [7,9]. Two other kinases participate in regulating exflagellation; namely, mitogen-activated protein kinase-2 (MAP2) is

* Corresponding author at: Department of Protozoology, Institute of Tropical Medicine (NEKKEN), Nagasaki University, 1-12-4 Sakamoto, Nagasaki 852-8523, Japan.

E-mail addresses: takahiro.ishizaki.0616@gmail.com (T. Ishizaki), chaiyawong.nat@gmail.com (N. Chaiyawong), hassanhakimi@gmail.com (H. Hakimi), masada@obihiro.ac.jp (M. Asada), mtachi@m.ehime-u.ac.jp (M. Tachibana), tishino@m.ehime-u.ac.jp (T. Ishino), kyahata@nagasaki-u.ac.jp (K. Yahata), okaneko@nagasaki-u.ac.jp (O. Kaneko).

<https://doi.org/10.1016/j.parint.2020.102056>

Received 31 December 2019; Received in revised form 12 January 2020; Accepted 13 January 2020

Available online 14 January 2020

1383-5769/© 2020 The Author(s). Published by Elsevier B.V. This is an open access article under the CC BY license (<http://creativecommons.org/licenses/by/4.0/>).

phosphorylated and activated by NIMA-related kinase-1 (NEK-1) and -3 (NEK3) [10,11], and is responsible for exflagellation and mosquito transmission [12]. Secondly, serine/arginine-rich protein kinase (SRPK), for which a deletion mutant in *P. berghei* showed normal morphology, but exflagellation was abolished [13].

Pseudokinases lack one or several catalytic residues, but still have significant roles in signaling pathways, such as binding to and modulating functions of other kinases and phosphatases, and competing with signal-related molecules by binding to their substrates [14]. Several pseudokinases have been characterized in apicomplexan parasites. In *Toxoplasma gondii*, a pseudokinase TgBPK1 is involved in cyst wall formation and infectivity to the host [15]. Another pseudokinase TgROP5 forms a complex with TgROP17 and TgROP18 kinases, which interact with host immunity-related GTPases (IRG) and regulate acute symptoms [16,17]. Malaria parasites possess 8 pseudokinases [18], all of which are poorly characterized with the exception of one pseudotyrosine kinase which was reported to be an exported protein to the infected erythrocyte and has a scaffolding role for serine repeat antigen 5 (SERA5) and protein phosphatase type 1 (PP1) [19].

Plasmodium yoelii PY17X_1220300 is a pseudokinase which is highly transcribed at the schizont and male gametocyte stages. Disruption of its ortholog in *P. berghei* (PBANKA_1217100) showed a slow growth phenotype during asexual replication in mice [20]. An exhaustive mutagenesis analysis suggested that its ortholog in *P. falciparum* (PF3D7_0321400) also has a slow growth phenotype in *in vitro* culture conditions [21,22]. To further characterize the role of this pseudokinase we took advantage that it is dispensable during the asexual stage, and evaluated PY17X_1220300 for its expression using epitope-tagged transgenic *P. yoelii* lines and its biological roles in the asexual and gametocyte stages using gene deletion parasite lines.

2. Experimental procedures

2.1. *In silico* protein analysis

Multiple sequence alignments were generated by the MAFFT software program using amino acid sequences retrieved from the PlasmoDB database [23,24]. Sequences used were *P. yoelii* PY17X_1220300, PY17X_0410700 (PyCDPK3), PY17X_0617900 (PyCDPK4), PY17X_0839000 (PyPKAc), PY17X_0412900, (PyGSK3), PY17X_0935700 (PyMAPK2), PF3D7_0321400, PRCDC_0320700, PBANKA_121700, PCHAS_1217800, PmUG01_08034700, PocGH01_0802710, PGAL8A_00394900, PKNH_0819400, and PVX_095165. Prediction of endoplasmic reticulum signal sequences, transmembrane regions, and nuclear transport signals were performed by SignalP ver 5.0, TMHMM ver 2.0, and SeqNLS, respectively [25–27]

2.2. Parasites and experimental animals

The *P. yoelii* 17XL line was maintained in 6–8 week old female ICR or BALB/c mice (Japan SLC, Hamamatsu, Japan). Animal experiments were approved by the Animal Care and Use Committee of Nagasaki University (Permit number: 1403031120–5).

2.3. Plasmid construction and transfection

A CRISPR/Cas9 plasmid (pDC2-Cas9-gRNA-hdHFR, a kind gift from the Wellcome Genome Campus Advanced Course) [28], was digested with BamHI, and then a DNA fragment containing the *P. yoelii* U6 promoter and its terminator PCR-amplified from *P. yoelii* gDNA was ligated using an In-Fusion HD cloning kit (Takara Bio Inc., Shiga, Japan), yielding pDC2-cam-Cas9-PyU6-hdHFR. To generate plasmids to knockout the PY17X_1220300 gene locus or to tag the C-terminal end with Myc epitopes, pDC2-cam-Cas9-PyU6-hdHFR was digested with *Bbs*I and ligated with the gRNA component targeting PY17X_1220300. The plasmid was then digested with *Hpa*I and *Aat*II and DNA fragments

for the 5'- and 3'-homologous recombination regions of Py17X_1220300 PCR-amplified from *P. yoelii* gDNA and hdHFR or hdHFR/yFCU expression cassettes PCR-amplified from pDC2-cam-Cas9-PyU6-hdHFR plasmid or p230p-TRAD4-Rand-mCherry plasmid (kind gift from Dr. Soldati), respectively, were ligated using an In-Fusion HD cloning kit, yielding pDC2-Cas9-PyU6-ΔPypPK1 and pDC2-Cas9-PyU6-PypPK1-myc, respectively. All primers used to generate plasmids are shown in the supplemental table S1. The plasmids for transfection were prepared using a HiSpeed Plasmid Midi Kit (Qiagen, Hilden, Germany).

Transfection to *P. yoelii* was performed as described with minor modification [29]. Schizonts were enriched by density gradient centrifugation using the Histodenz solution (1.077 g/mL) and were mixed with human T cell nucleofector solution (Lonza, Basel, Switzerland) containing 20 µg of the circular plasmids and electroporated using a Nucleofector™ 2b device (Lonza; U-33 program). Drinking water containing 0.07 g/mL pyrimethamine (Fukuzyu Pharmaceutical Co., LTD, Japan) was administered orally from one day post transfection and parasites emerged following drug selection were passaged to a new mouse, then cloned by limiting dilution. To confirm the gene deletion and the insertion of the epitope tag sequence, gDNA of transfectants were extracted using a QIAamp DNA Blood Mini Kit (Qiagen), and PCR was performed with specific diagnostic primer pairs (Table S1), because off-target effects have not been reported [30].

2.4. Gametocyte preparation and ookinete induction

Wild type or ΔPypPK1 parasite-infected blood was collected by cardiac puncture and the gametocyte-enriched fraction (together with schizonts) was obtained by Histodenz density gradient centrifugation described above. To induce gametogenesis, fertilization, and ookinete transformation, enriched gametocytes were incubated for 16 h at 24 °C in ookinete culture medium (RPMI1640 medium supplemented with 0.225% sodium bicarbonate, 20% fetal calf serum, 25 mM HEPES, 50 µg/mL hypoxanthine, and 100 µM xanthurenic acid (XA)) [31]. The ookinete fraction was enriched by density gradient centrifugation as described above.

2.5. Western blot analysis

Schizonts were enriched by Histodenz density gradient centrifugation and treated with saponin in PBS containing protease inhibitor cocktail (PBS-PI; cOmplete™ EDTA-free, Sigma-Aldrich). Saponin-lysed pellets were washed with PBS-PI and lysed with 1% Triton X-100 in PBS-PI for 30 min on ice. To obtain gametocyte materials without asexual stage parasites, drinking water containing 10 mg/L of sulfadiazine was administered to parasite-infected mice for 2 days before blood collection. Gametocytes were enriched by density gradient centrifugation described above and proteins were extracted from 5×10^7 gametocytes with 1% Triton X-100/PBS-PI. Extracted proteins were subjected to electrophoresis on a 5–20% SDS-polyacrylamide gradient mini gel (ATTO, Tokyo, Japan), then transferred onto PVDF membranes (Millipore, Billerica, MA). Membranes were probed with mouse anti-Myc monoclonal antibody (1:1000 dilution; 9B11; Cell Signaling Technology, Danvers, MA), rabbit anti-PyAMA1 polyclonal antibody (1:300 [29]), rabbit anti-α-tubulin II serum (1:1000; *P. falciparum* [32]), or mouse anti-PyS25 antibody (1:100 [31]). Horseradish peroxidase (HRP)-conjugated anti-mouse IgG or anti-rabbit IgG (1:8000; Promega, Madison, WI) were used as secondary antibodies. Bands were detected with Immobilon Western Chemiluminescent HRP substrate (Millipore) and images were captured by a chemiluminescence detection system (LAS-4000EPUVmini with Multi Gauge software; Fujifilm, Japan).

2.6. Indirect immunofluorescent assay (IFA)

Thin blood smears of *P. yoelii* were fixed with 4% paraformaldehyde and 0.075% glutaraldehyde (PFA-GTA) in PBS for 15 min at room

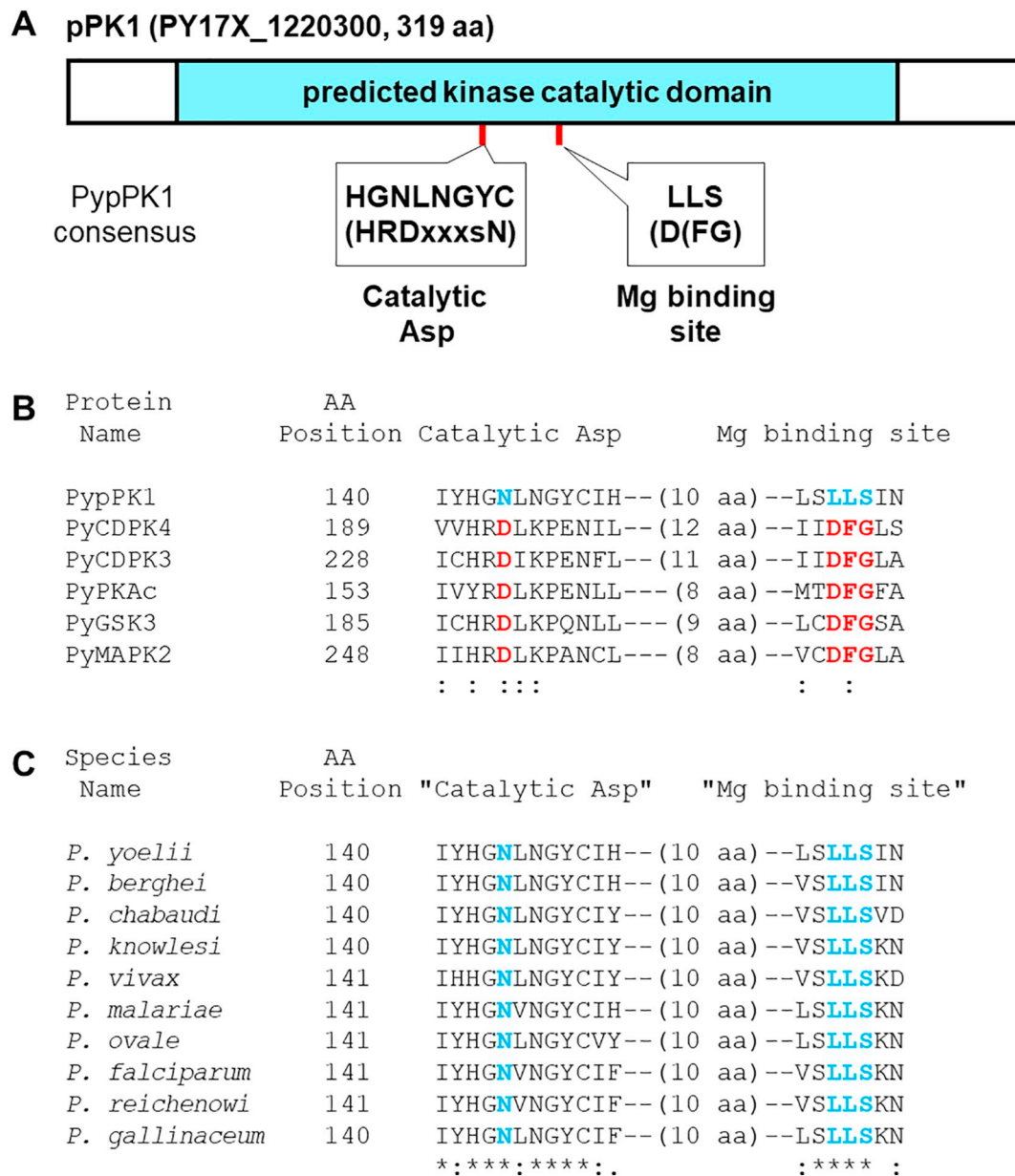


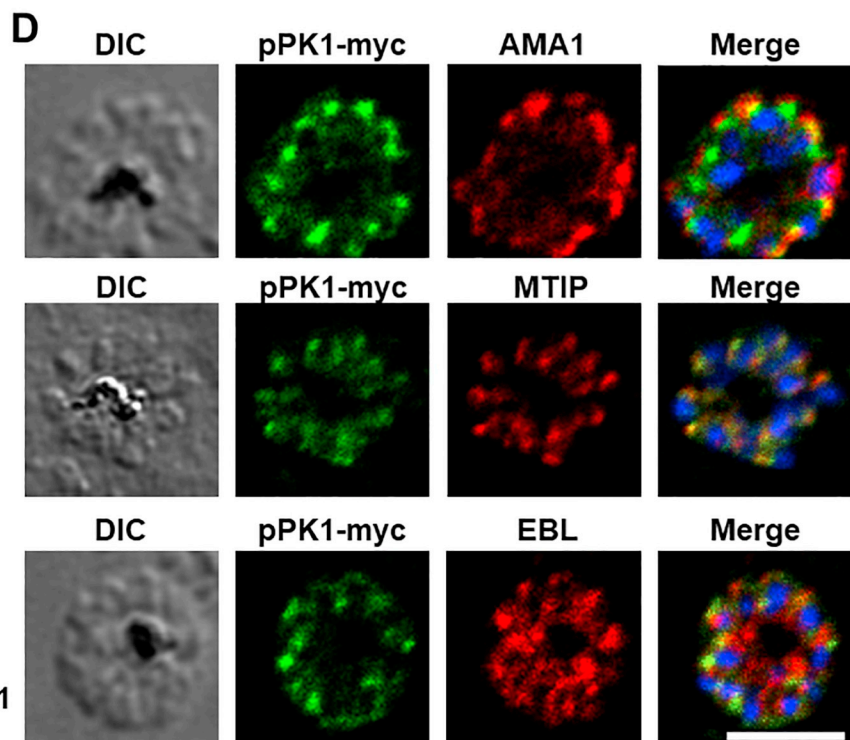
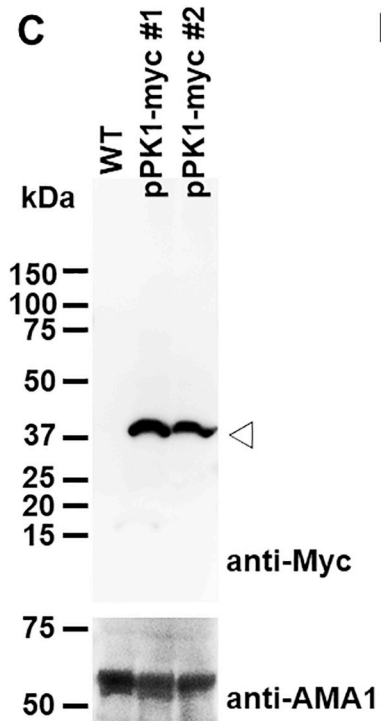
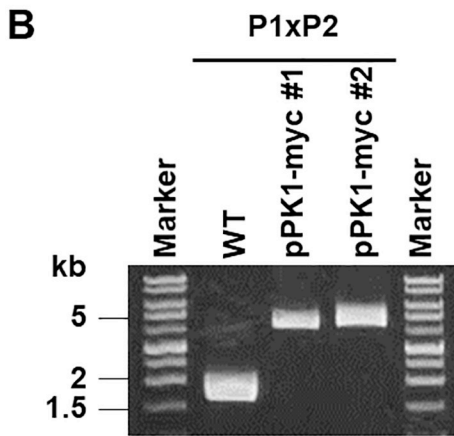
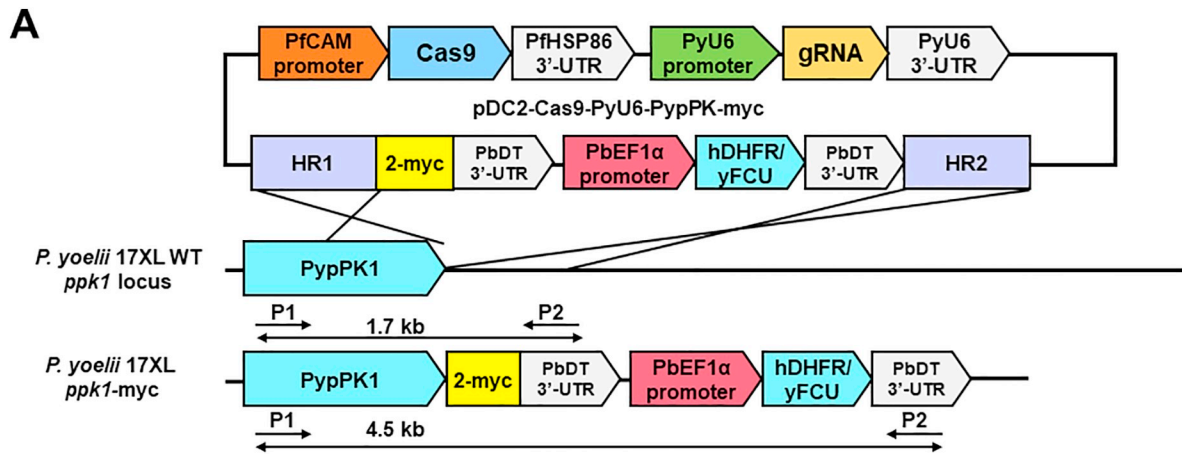
Fig. 1. PypPK1 lacks a catalytic aspartate and a Mg binding site. (A) A schematic image of *P. yoelii* pPK1 domain structure. Shown are the kinase catalytic domain predicted by CD-search and the consensus sequences for the catalytic aspartate and the Mg binding site. (B and C) Amino acid alignments of sequences around the catalytic aspartate and the Mg binding domain of PypPK1 with other *P. yoelii* kinases (B) or PypPK1 orthologs in other *Plasmodium* spp. (C). Critical amino acid residues matching to the consensus residues are shown in red, and non-matching residues are shown in blue. (For interpretation of the references to colour in this figure legend, the reader is referred to the web version of this article.)

temperature (RT). The smears were permeabilized with 0.1% Triton X-100/PBS for 10 min at RT, then washed extensively with PBS. Smears were blocked with 3% BSA/PBS for 1 h at RT, immunostained with primary antibodies, and incubated for 1 h at RT. Primary antibodies were mouse or rabbit anti-Myc monoclonal antibodies (1:500; 9B11 or 71D10, respectively, Cell Signaling Technology), rabbit anti-PyAMA1 (1:250; microneme marker [33]), rabbit anti-PyEBL (1:250; dense granule marker [34]), rabbit anti-PbMTIP (1:250; inner membrane complex marker), rabbit anti- α -tubulin II serum (1:1000; male gametocyte marker [32]), or mouse anti-Pys25 antiserum (1:20; female gametocyte marker [31]). Smears were then incubated for 30 min at RT with Alexa fluor 488 or 594-conjugated goat anti-mouse or rabbit IgG secondary antibodies (1:1000; Invitrogen) and 4',6-diamidino-2-phenylindole (DAPI; Invitrogen, Carlsbad, CA) and mounted with antifade mounting medium (VECTAS-HIELD; Vector laboratories, Burlingame, CA). Images were obtained using a confocal microscope system (A1 Rsi; Nikon, Tokyo, Japan).

To evaluate protein expression on the surface of purified merozoites and microgametes, the samples were fixed with PFA-GTA for 15 min and placed onto poly-L-lysine-coated cover glasses for 30 min [29]. Cover glasses were incubated with 3% BSA/PBS at RT for 1 h, then with primary antibodies at RT for 1 h, and finally with secondary antibodies at RT for 30 min. Antibodies used for merozoites were chicken anti-PyMSP1 antibody (1:500; [35]), rabbit anti-PyAMA1 antibody (1:250), and rabbit anti-PyEBL antibody (1:250). Antibodies for microgametes were rabbit anti-PyMiGS antibody (1:1000 [31]), rabbit anti-PyS230 antibody (1:100, Fig. S2), and rabbit anti- α -tubulin II serum (1:1000). All images were obtained as described above.

2.7. RNA isolation, cDNA synthesis, and reverse-transcription polymerase chain reaction (RT-PCR)

Parasite total RNA was extracted using TRIzol (Thermo Fisher, Waltham, MA) and SV total RNA isolation system (Promega) following



(caption on next page)

Fig. 2. Generation of *P. yoelii* pPK1-myc parasites. (A) A schematic image of a plasmid to generate *P. yoelii* 17XL expressing Myc-tagged pPK1. Location of primers P1 and P2 and the expected size of PCR products are indicated. WT, wild type; PFCAM; *P. falciparum* calmodulin, PfHSP86; *P. falciparum* heat shock protein 86, PyU6; *P. yoelii* U6; PbDT; *P. berghei* dihydrofolate reductase thymidylate synthase, PbEF1 α ; *P. berghei* elongation factor 1 α , hDHFR; human DHFR. (B) Diagnostic PCR to confirm Myc-tag sequence insertion. (C) Western blot with anti-Myc or anti-AMA1 antibodies. Approximately 40-kDa bands detected with anti-Myc antibodies are indicated with a white arrowhead. AMA1 served as a loading control. (D) PypPK1 localization with marker proteins. Fluorescent signals with anti-Myc antibody (green, pPK1-myc) were merged with differential interference contrast (DIC) images, DAPI nucleus signals (blue), and marker protein signals (red: AMA1, microneme marker; EBL, dense granule marker; or MTIP, inner membrane complex marker). (For interpretation of the references to colour in this figure legend, the reader is referred to the web version of this article.)

the manufacturers' protocols. Complementary DNA (cDNA) synthesis was carried out using SuperScript III reverse transcriptase (Invitrogen) and random hexamers according to the company's instruction. RT-PCR was performed with primers listed in the table S1 using Tks Gflex polymerase (Takara Bio Inc.). *Pypkac* was used as a positive control.

2.8. Asexual parasite growth assay and mouse survival assay

Parasite-infected erythrocytes (10^6) were intravenously injected into mice (6-weeks old female BALB/c, $n = 5$) and parasitemias were monitored daily by microscopic observation of Giemsa-stained thin blood smears. To determine parasitemias, at least 10,000 erythrocytes or 100 parasites were counted and differences were examined by one-way ANOVA followed by a post-hoc Tukey's multiple comparison test using Prism 6 software (GraphPad Software Inc., San Diego, CA). To evaluate parasite virulence, 10^6 parasite-infected erythrocytes were intravenously injected into mice (6-week old female BALB/c, $n = 10$), then survival was monitored every day up to 14 days post-inoculation. Mouse survival rates were shown as Kaplan-Meier curves and significant differences were evaluated by the Log-rank (Mantel-Cox) test implemented in Prism 6 software. To examine erythrocyte preference, selectivity index (SI) was calculated as described [36].

2.9. In vitro and in vivo erythrocyte invasion assay

In vitro invasion assays were performed as described [29]. In brief, 10^7 enriched schizonts described above were resuspended in complete culture medium for *P. yoelii* (PyCM: RPMI1640 medium supplemented with 0.225% sodium bicarbonate, 1% AlbuMax I, 25 mM HEPES, 50 μ g/mL hypoxanthine, and 10 μ g/mL gentamicin) and free merozoites were obtained by filtration through a filter unit (1.2 μ m pore size; Sartorius Stedim Biotech, Göttingen, Germany) at 15 °C. Purified free merozoites (approximately 1×10^6) were mixed with uninfected mouse erythrocytes pre-warmed to 37 °C (approximately 5×10^6) in 300 μ L of PyCM and incubated with 5% O₂, 5% CO₂, and 90% N₂ gas mixture at 37 °C for 1 h using a shaking incubator at 1000 rpm. Mixtures were then centrifuged, and the pellets resuspended with fresh PyCM to a final hematocrit of 1.66% and transferred to a 96-well plate. Parasites were further incubated for 18 h with the above-mentioned gas mixture. Giemsa-stained blood smears were prepared and at least 10,000 erythrocytes were counted to calculate parasitemia. Significant differences were evaluated by one-way ANOVA followed by Tukey's multiple comparison test.

For *in vivo* invasion assays, 10^8 enriched matured schizonts were intravenously inoculated into mice ($n = 5$) and parasitemias were monitored independently for each stage by microscopic examination of Giemsa-stained blood smears at 2 h post-inoculation. At least 10,000 erythrocytes were counted to calculate parasitemia and significant differences were evaluated by Kruskal-Wallis one-way ANOVA followed by Dunn's multiple comparison test using Prism 6 software.

2.10. Evaluation of gametocytemia

To evaluate gametocytogenesis 10^6 parasites were inoculated into mice (BALB/c, $n = 3$) and thin blood smears were prepared on day 3 post-inoculation. The smears were probed with rat anti-TER-119 antibody (1:500; Medical & Biological Laboratories, Tokyo, Japan), rabbit anti- α -tubulin II antibody, or mouse anti-Pys25 antiserum, then reacted with Alexa fluor 488-conjugated goat anti-rat IgG, Alexa fluor 568-

conjugated goat anti-rabbit IgG, or Alexa fluor 647-conjugated goat anti-mouse IgG secondary antibodies, respectively. Blocking, reaction, and data acquisition were performed as described in section 2.6. At least 10,000 erythrocytes were counted to determine gametocytemia.

2.11. Assays to evaluate gametocyte egress, exflagellation, and oocyst numbers

Gametocyte egress assays were performed as described [31]. Briefly, gametocytes were enriched as described in section 2.5 and gametocyte egress was induced by incubating in ookinete culture medium containing XA. After 15 or 30 min incubation, cultures were fixed with PFA and thin blood smears were prepared to evaluate male or female gametocyte egress, respectively. The blood smears were immunostained with anti-TER-119 (erythrocyte marker), α -tubulin II antiserum (male gametocyte/microgamete marker), and anti-Pys25 antiserum (female gametocyte/macrogamete marker). The male or female gametocyte egress ratios were obtained by dividing the number of parasites with α -tubulin II- or Pys25-positive and TER-119 negative by the number of α -tubulin II- or Pys25-positive parasites, respectively. To quantitate exflagellation, 3 μ L of parasite-infected blood was resuspended in 57 μ L of ookinete culture medium and incubated at RT for 5 min. The mixture was then applied to a hemocytometer and the number of exflagellation centers per 1×10^4 erythrocytes were counted from day 2 to 4 post-infection [31]. The numbers of exflagellated male gametocytes were estimated from male gametocytemia, egress ratio, and exflagellated ratio at day 3. Then, the observed numbers of exflagellation centers were divided by the estimated number of exflagellated male gametocytes. The ratio of exflagellation centers per exflagellated male gametocyte were normalized by the average of the pPK1-myc parasites. Significant differences in gametocyte egress ratios, exflagellation ratios, and the number of exflagellation centers were evaluated by one-way ANOVA followed by Tukey's multiple comparison test. *Anopheles stephensi* mosquitoes were fed on parasite-infected ICR mice. Fully engorged mosquitoes were maintained at 24 °C with a 12 h light/dark cycle. The number of midgut oocysts was counted from at least 35 mosquitoes under the microscope on day 11 post-feeding [37] and significant differences were evaluated by Kruskal-Wallis one-way ANOVA followed by Dunn's multiple comparison test.

2.12. Time lapse imaging of exflagellation

Blood from parasite-infected mice were collected from tail veins on day 3 post-inoculation, mixed with ookinete culture medium, applied to C-Chip hemocytometer slides (NanoEnTek Inc., Seoul, South Korea), and observed using a confocal microscope system (A1 Rsi; Nikon) with a 60 \times magnification lens. Video images were obtained every 0.1 s, up to 20 min using a CCD camera (ORCA-R2), cropped, and analyzed using Fiji software [38].

3. Results

3.1. PypPK1 is conserved among Plasmodium spp. and lacks a catalytic aspartate and a Mg binding site

PY17X_1220300 encodes a 319 amino acid protein with an expected molecular weight of 38 kDa. The CD-Search webware predicted a protein kinase catalytic domain from amino acid positions (aa) 36 to 278 (E -value = $6.63e^{-22}$; Fig. 1A) [39], and a signal peptide sequence or transmembrane region was not predicted [25,26]. An active protein kinase has

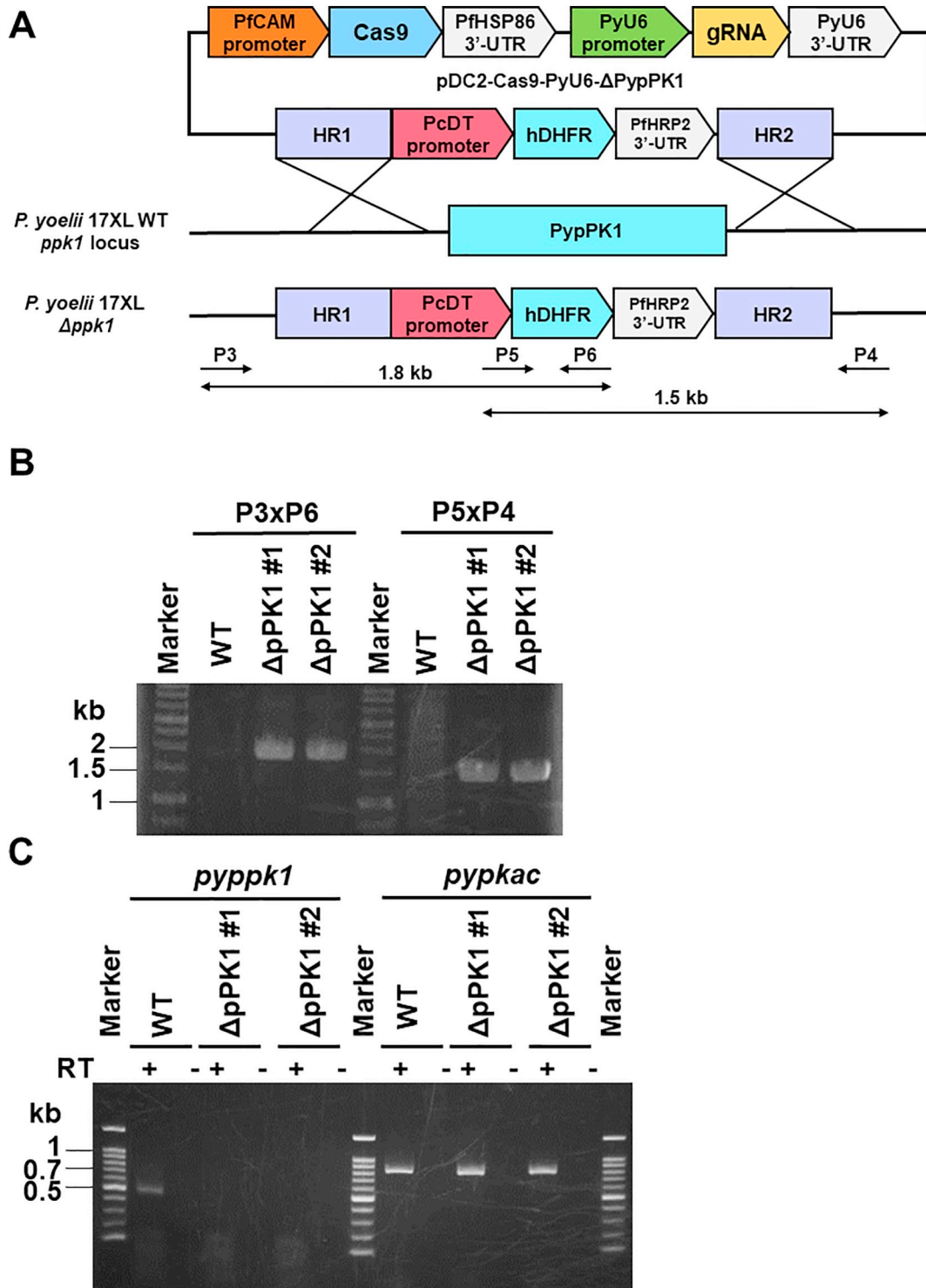


Fig. 3. Generation of *P. yoelii* $\Delta pPK1$ parasites. (A) A schematic image of a plasmid to delete the pPK1 gene locus in *P. yoelii* 17XL. Location of primers P3, P4, P5, and P6 and the expected size of PCR products are indicated. PcDT; *P. chabaudi* dihydrofolate reductase thymidylate synthase; PfHRP2; *P. falciparum* histidine-rich protein 2. Others are described in the Fig. 2 legend. (B) Diagnostic PCR to confirm the gene deletion in $\Delta pPK1$ parasites. (C) RT-PCR to confirm mRNA depletion in $\Delta pPK1$ parasites. Primers targeting *pyppk1* or *pypkac* were used. RT; reverse transcriptase.

several critical features for phosphorylation activity such as a catalytic aspartate and a Mg binding site. The corresponding regions of PY17X_1220300 were not conserved with the known *P. yoelii* protein kinases, PyCDPK4, PyCDPK3, PyPKAc, PyGSK3, and PyMAPK2, suggesting that PY17X_1220300 does not possess phosphorylation activity (Fig. 1B). The relevant regions are widely conserved within orthologs in other *Plasmodium* spp. (Fig. 1C and Fig. S1), suggesting that PY17X_1220300 is a pseudokinase

with a conserved role across *Plasmodium*. Taken together, we designated this protein as *P. yoelii* pseudo Protein Kinase 1 (PypPK1).

3.2. PypPK1 is localized at the apical side of daughter merozoites

Myc epitope tags were introduced at the C-terminus of PypPK1 via homologous recombination and the resulting pPK1-myc transgenic *P.*

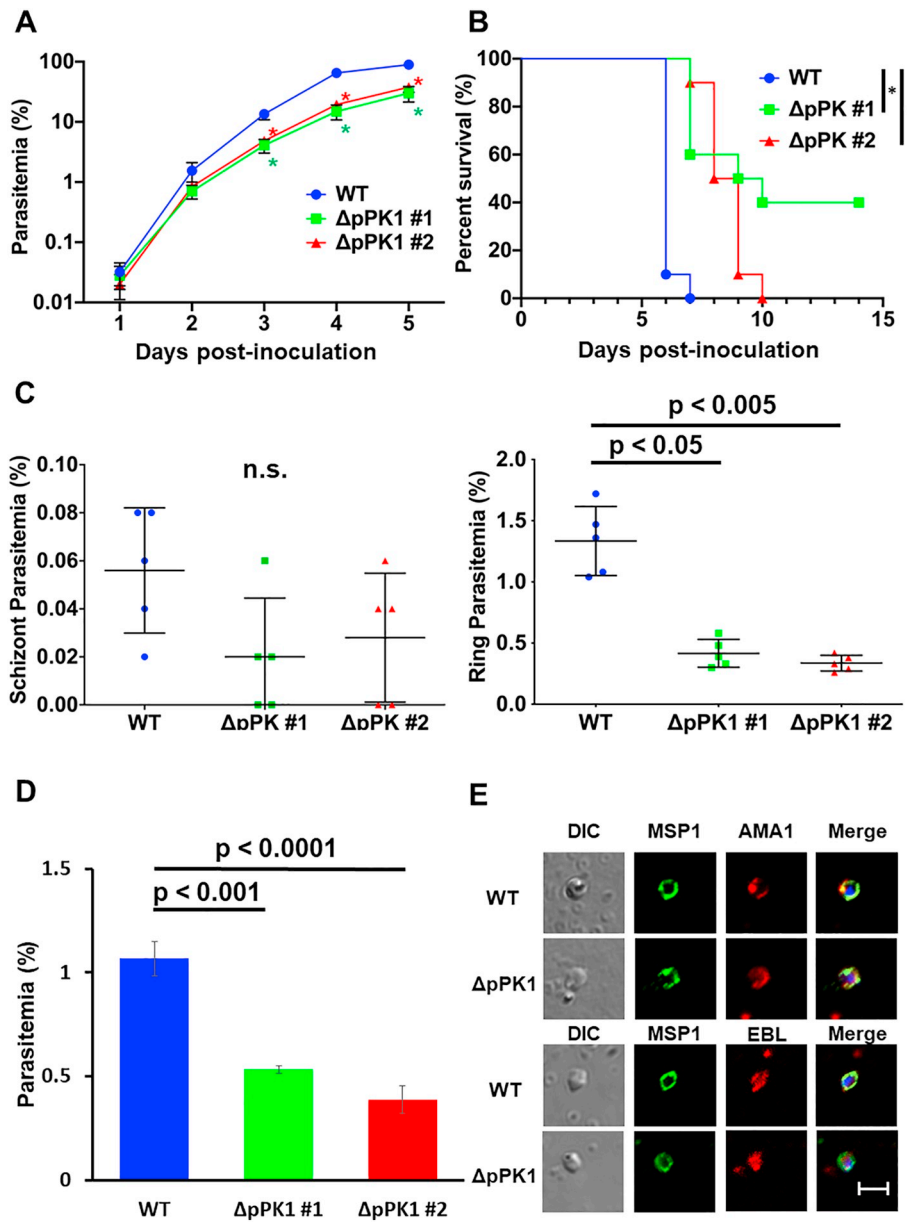


Fig. 4. Phenotypes of $\Delta pPK1$ parasites during asexual stage development. (A) Parasitemia curves of wild type (WT) parasites and two $\Delta pPK1$ parasite clones #1 and #2 ($n = 5$). Parasitemias were monitored every day after inoculation of 1×10^6 parasites. Asterisks indicate that the $\Delta pPK1$ parasitemia was significantly higher than WT parasitemia at each examined day ($p < .01$ by Tukey's multiple comparison test). (B) Kaplan-Meier curves with 10 BALB/c mice for each group. Mouse survival rates with $\Delta pPK1$ parasites were significantly higher than for WT parasites ($* p < .001$ by Mental-Cox test). (C) *in vivo* erythrocyte egress and invasion assay. Egress efficacy and parasite invasion ability was evaluated by schizont (left) and ring (right) stage parasitemias at 2 h post inoculation of 1×10^8 schizonts into a mouse. Ring stage parasitemias of $\Delta pPK1$ #1 and #2 parasites were significantly lower than that of WT parasites by Dunn's multiple comparison test). n.s.; not significant. (D) *in vitro* erythrocyte invasion assay. The invasion efficacy of $\Delta pPK1$ parasites was significantly lower than that of WT parasites by Tukey's multiple comparison test. (E) Microorganelle protein secretion assay for WT and $\Delta pPK1$ #1. DIC, differential interference contrast image; MSP1 merozoite surface protein 1 (green); AMA1 or EBL (red). MSP1 and AMA1 or EBL images were merged with DAPI nucleus signals (Merge). Scale bar 2 μm . (For interpretation of the references to colour in this figure legend, the reader is referred to the web version of this article.)

Table 1
Selectivity index.

Parasite	n	Selectivity index (range)	p value (vs WT)
Py17XL WT	5	1.79 (1.07–2.44)	
$\Delta pPK1$ #1	5	2.97 (1.84–4.65)	n.s.
$\Delta pPK1$ #2	5	3.03 (2.06–4.25)	n.s.

WT = wild type. n.s. = not significant.

yoelii clones were verified by diagnostic PCR (Fig. 2A and B). Western blot analysis of pPK1-myc clones with anti-Myc antibody revealed a single band around 40 kDa, consistent to the calculated molecular weight of this protein, 40.2 kDa (Fig. 2C). Protein extracts from wild type parasites did not show any bands, thus excluding non-specific reaction of the anti-Myc antibody. Western blot analysis using anti-AMA1 antibody ensured that the loaded protein amounts were similar (Fig. 2C bottom). IFA of pPK1-myc schizont-stage parasites showed that pPK1-myc signals were more closely co-localized with signals for the microsome marker AMA1 and the inner membrane complex marker MTIP than the signal for the dense granule marker EBL (Fig. 2D). These

results suggest that pPK1-myc is expressed at the schizont stage of *P. yoelii*, consistent to the peak transcription pattern at this stage of *P. berghei* during the asexual cycle, and localized at the apical side of each daughter merozoite.

3.3. Deletion of pPK1 reduced *P. yoelii* activity to invade host erythrocytes and its virulence

To examine the function of pPK1, two clones of *P. yoelii* pPK1 deletion mutants ($\Delta pPK1$ #1 and #2) were independently generated using CRISPR/Cas9 methodology (Fig. 3A). Deletion of the pPK1 gene locus and the loss of mRNA were confirmed by diagnostic PCR and RT-PCR, respectively (Fig. 3B and C). $\Delta pPK1$ parasites showed a significant growth defect and a significant number of mice infected with this parasite survived longer than mice infected with the wild type parasite (Fig. 4A and B). Because pPK1 is expressed in daughter merozoites, we examined the effect on erythrocyte egress and invasion by parasites. Firstly, fully matured schizonts were purified and injected into mice and non-egressed schizonts and newly invaded ring stage parasites were monitored 2 h later by microscopic observation of Giemsa-stained blood

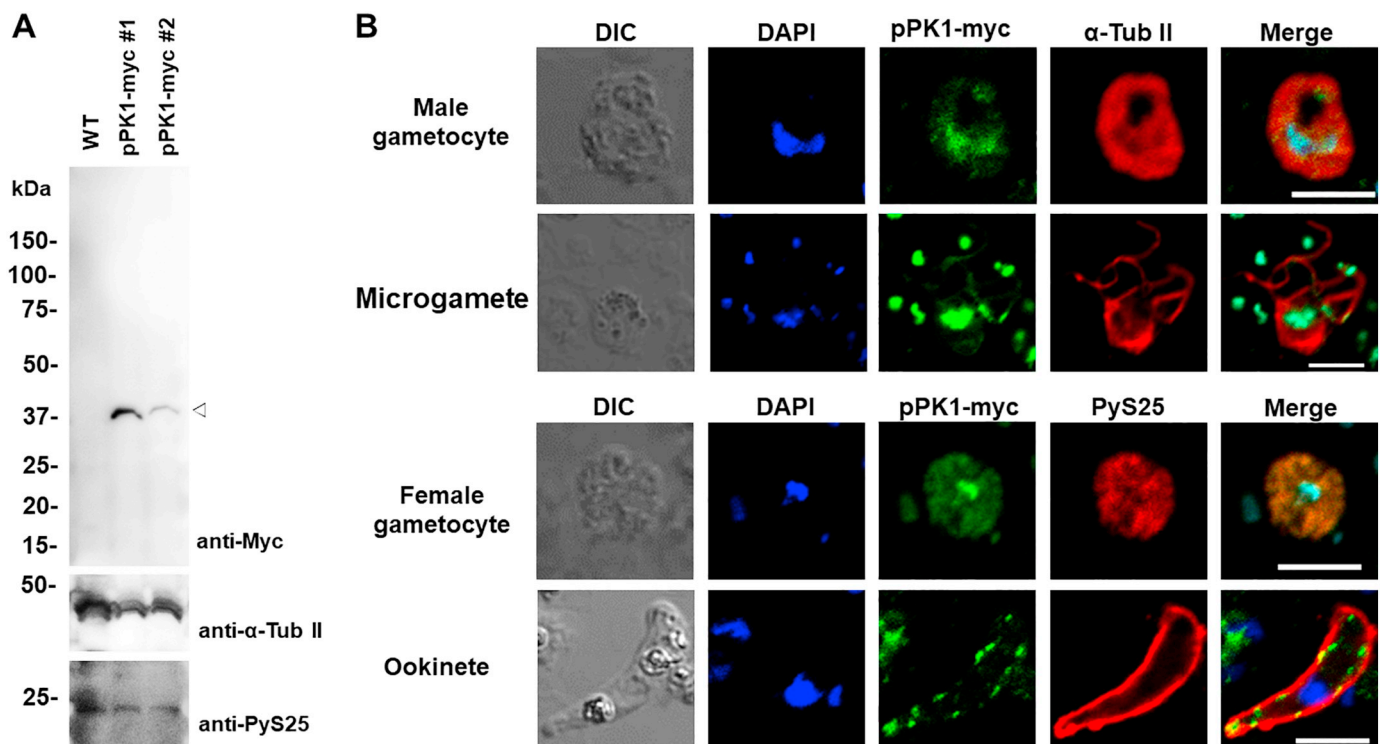


Fig. 5. PypPK1 was detected at sexual stages. (A) Western blot for gametocytes of wild type and pPK1-myc parasites with anti-Myc, anti- α -tubulin II (α -Tub II, male marker), and anti-PyS25 (female marker) antibodies. White arrowhead indicates a band detected with anti-Myc antibody. (B) IFA images of PypPK1 at male and female gametocytes, microgametes, and ookinete stages stained with anti-Myc (green) and anti- α -Tub II or anti-PyS25 (red). PypPK1-myc signals and α -tubulin II or PyS25 signals were merged with DAPI (blue) nucleus signals (Merge). Scale bars, 5 μ m. (For interpretation of the references to colour in this figure legend, the reader is referred to the web version of this article.)

smears. The percentage of non-egressed schizonts was not significantly different between wild type and Δ pPK1 parasites (Fig. 4C left); however, the ratio of newly invaded ring stages of Δ pPK1 parasites was significantly lower than for wild type parasites (Fig. 4C right). In addition, *in vitro* erythrocyte invasion assays revealed that the parasitemias of Δ pPK1 #1 and #2 parasites were $0.53 \pm 0.02\%$ and $0.39 \pm 0.08\%$, respectively, significantly lower than the parasitemia of the parental wild type parasites ($1.07 \pm 0.10\%$) (Fig. 4D). These *in vivo* and *in vitro* results indicate that pPK1 is not crucial for erythrocyte egress, but partly contributes to erythrocyte invasion.

To investigate whether the reduction in erythrocyte invasion efficiency is due to an altered erythrocyte preference by Δ pPK1 parasites, a selectivity index (SI) was calculated at day 3 post-inoculation (Table 1). The SI value of parasites that can only invade immature erythrocytes is high (e.g. *P. yoelii* 17XNL and *P. vivax*), whereas the SI value of parasites that invade both immature and mature erythrocytes is low (e.g. *P. yoelii* 17XL and *P. falciparum*) [34,36]. The SI value of Δ pPK1 #1 and #2 parasites were 2.97 and 3.03, respectively, slightly higher than the value of wild type parasites (1.79), but the difference was not significant. Thus, the effect of PypPK1 gene deletion on erythrocyte preference appears to be marginal or absent.

Because phosphorylation signals are involved in organelle discharge, we investigated whether depletion of pPK1 affected the secretion of two invasion related organelle molecules, AMA1 and EBL [29,40]. Signals of both proteins were detected on the merozoite surface of wild type and Δ pPK1 parasites (Fig. 4E), suggesting that pPK1 has no or a limited role in AMA1 and EBL secretion in the *P. yoelii* 17XL line.

3.4. pPK1 plays an important role for exflagellation center formation

Next, we examined the expression of pPK1 in sexual stage parasites using pPK1-myc parasites. Western blot analysis was performed for

enriched gametocytes from mice treated with sulfadiazine for 2 days before collection. Only a few asexual stage parasites (< 1% of gametocytes) were observed by microscopy after sulfadiazine treatment. A single ~40-kDa band, similar to the band from asexual stage parasites, was detected with anti-Myc antibody (Fig. 5A). IFA against α -tubulin II-positive male and PyS25-positive female gametocytes revealed that pPK1-myc fluorescent signals overlapped with the DAPI-nucleus signals in both gametocytes. The fluorescent signal was also detected at the nucleus of microgametes (Fig. 5B). A patchy fluorescent pattern was detected along the ookinete plasma membrane and in this parasite stage the pPK1-myc signals did not overlap with nucleus signals (Fig. 5B). These data indicate that PypPK1 is expressed in sexual stage parasites and its localization differed among stages.

To investigate a role of pPK1 in sexual stage parasites, firstly gametocytemias were compared between pPK1-myc and Δ pPK1 parasites by counting immuno-stained parasites labeled with male and female gametocyte markers. Male gametocytemias of Δ pPK1 #1 and #2 parasites on day 3 post-infection were $0.08 \pm 0.03\%$ and $0.10 \pm 0.01\%$, respectively, which were not significantly different from that of pPK1-myc parasites ($0.11 \pm 0.03\%$). Female gametocytemias of Δ PypPK1 #1 and #2 parasites were $0.12 \pm 0.04\%$ and $0.11 \pm 0.03\%$, respectively, and the difference from the pPK1-myc parasites ($0.14 \pm 0.02\%$) was not significant (Fig. 6A). Secondly, we compared the ratio of gametocyte egress by counting male or female parasites within or outside the erythrocyte after XA activation. The signals of non-egressed gametocytes (with anti- α -tubulin II or anti-PyS25) were co-localized with the erythrocyte marker TER-119 signals, whereas the signals of egressed gametocyte were not co-localized with TER-119 signals (Fig. S3). The egress ratios were calculated for male and female gametocytes independently at 15 and 30 min post XA induction, respectively (Fig. 6B). Male gametocyte egress rates of Δ pPK1 #1 and #2 parasites were $54 \pm 4\%$ and $53 \pm 4\%$, respectively, which was not significantly different from that of pPK1-myc parasites

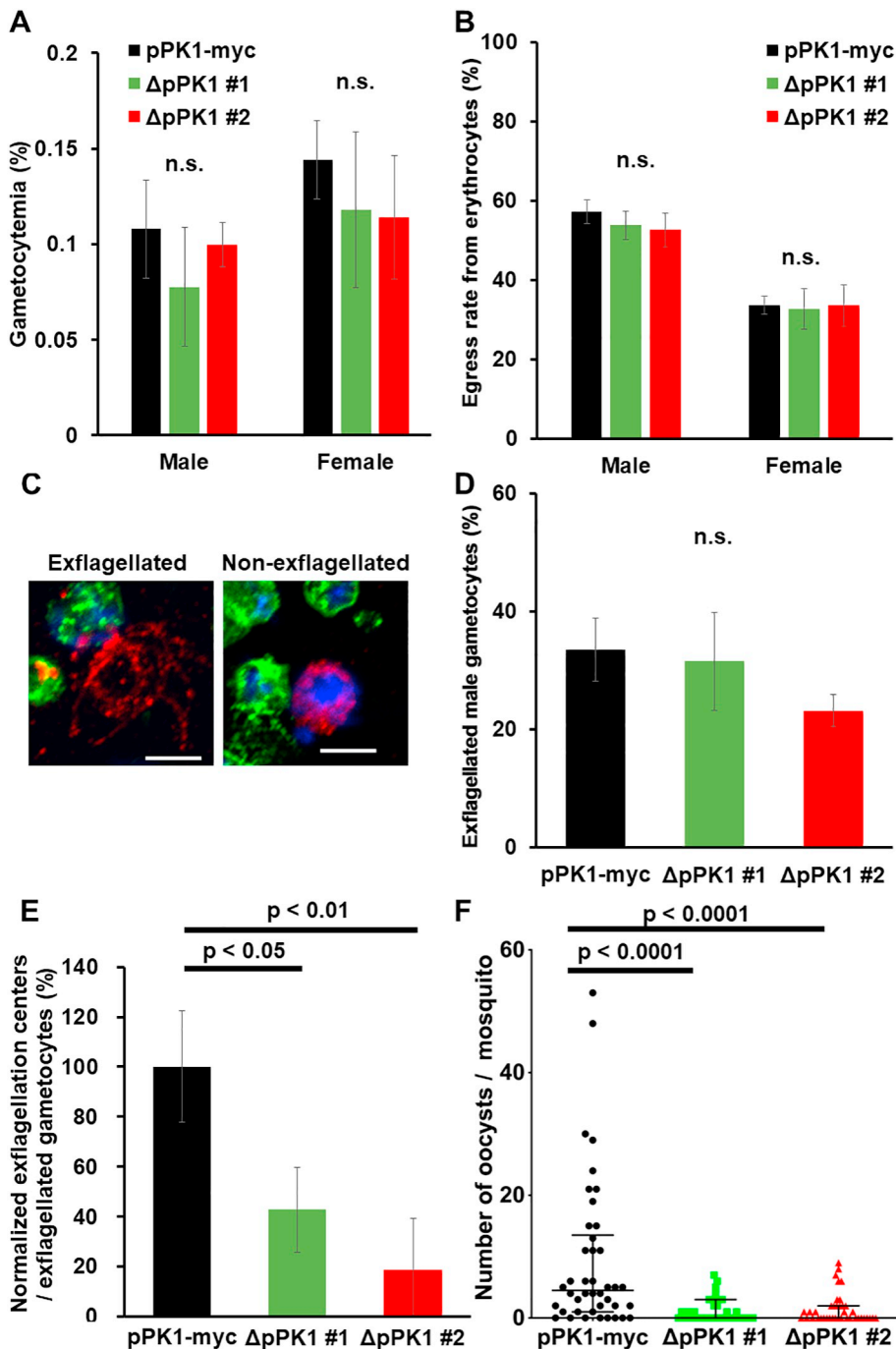


Fig. 6. Phenotypes of Δ pPK1 parasites during sexual stage development. (A) Male and female gametocytemias of pPK1-myc parasites and two Δ pPK1 clones. No significant difference (n.s.) was detected by one-way ANOVA test. (B) Male and female gametocyte egress rates from erythrocytes after XA activation. No significant difference (n.s.) was detected by one-way ANOVA test. (C) Images of exflagellated and non-exflagellated male gametocytes. Erythrocyte membrane, microgamete axonemes, and nuclei were detected with anti-TER-119 (green), anti- α -tubulin II (red), and DAPI (blue), respectively. (D) The ratio of exflagellated male gametocytes. The number of exflagellated parasites was divided by the number of egressed male gametocytes. No significant difference was detected by one-way ANOVA test. (E) Normalized percentage of exflagellation centers per exflagellated male gametocyte. The number of exflagellated male gametocytes were estimated from male gametocytemias, egress ratios, and exflagellation ratios at day 3. Then, the observed number of exflagellation centers were divided by the estimated number of exflagellated male gametocytes. Values were normalized by the average of the pPK1-myc parasites. Significant difference was detected by one-way ANOVA followed by Tukey's multiple comparison test. (F) The number of mosquito midgut oocysts. Mosquitoes were fed at day 3 after intravenous inoculation of 5×10^6 parasites to mice. Oocyst numbers were counted at day 11 post-feeding and shown with median and interquartile range. Significant difference was detected by one-way ANOVA followed by Dunn's multiple comparison test. The number of mosquitoes dissected for oocyst counting were 42 for pPK1-myc, 37 for Δ pPK1 #1, and 42 for Δ pPK1 #2. (For interpretation of the references to colour in this figure legend, the reader is referred to the web version of this article.)

(57 ± 3%). Female gametocyte egress rates of Δ pPK1 #1 and #2 parasites were 33 ± 5% and 34 ± 5%, respectively, and no significant difference was detected from that of pPK1-myc parasites (34 ± 2%). Egressed male gametocytes initiate three rounds of endomitosis to produce eight microgametes, followed by axoneme assembly and exflagellation to release eight motile male gametes [41]. Thus, thirdly, we evaluated exflagellation rates using the ratio of the number of exflagellated male gametocytes (Fig. 6C left) per the number of egressed male gametocytes (Fig. 6C right). The exflagellation rates of Δ pPK1 #1 and #2 parasites were 31.5 ± 8.4% and 23.1 ± 2.7%, respectively, and not significantly different from that of pPK1-myc parasites (33.4 ± 5.3%) (Fig. 6D). Fourthly, the effect on the exflagellation center formation was examined; that is, the clustering of exflagellating microgametes with surrounding erythrocytes. The number of exflagellation centers per erythrocyte at day 3 after parasite inoculation to

mice was normalized by the male gametocytemia, the egress rate, and the exflagellation rate (Fig. 6E). The normalized percentage of exflagellation centers per exflagellated male gametocyte were 43 ± 17 and 19 ± 21 for Δ pPK1 #1 and #2 parasites, respectively, significantly lower than the value for pPK1-myc parasites (100 ± 22%). Microscopic observation revealed that some Δ pPK1 parasites successfully formed exflagellation centers (Fig. 7A middle; Movie S2), and some Δ pPK1 parasites failed to form (Fig. 7A bottom; Movie S3), whereas the exflagellation center was always formed for wild type parasites (Fig. 7A top and Movie S1). Lastly, the number of mosquito midgut oocysts were compared between Δ pPK1 and pPK1-myc parasites. The numbers of oocysts per mosquito were counted at day 11 after blood feeding. The median and interquartile range of oocyst numbers of Δ pPK1 #1 and #2 parasites were 0.0 (0.0–3.0) and 0.0 (0.0–2.0), which were significantly lower than that of pPK1-myc parasites (4.5,

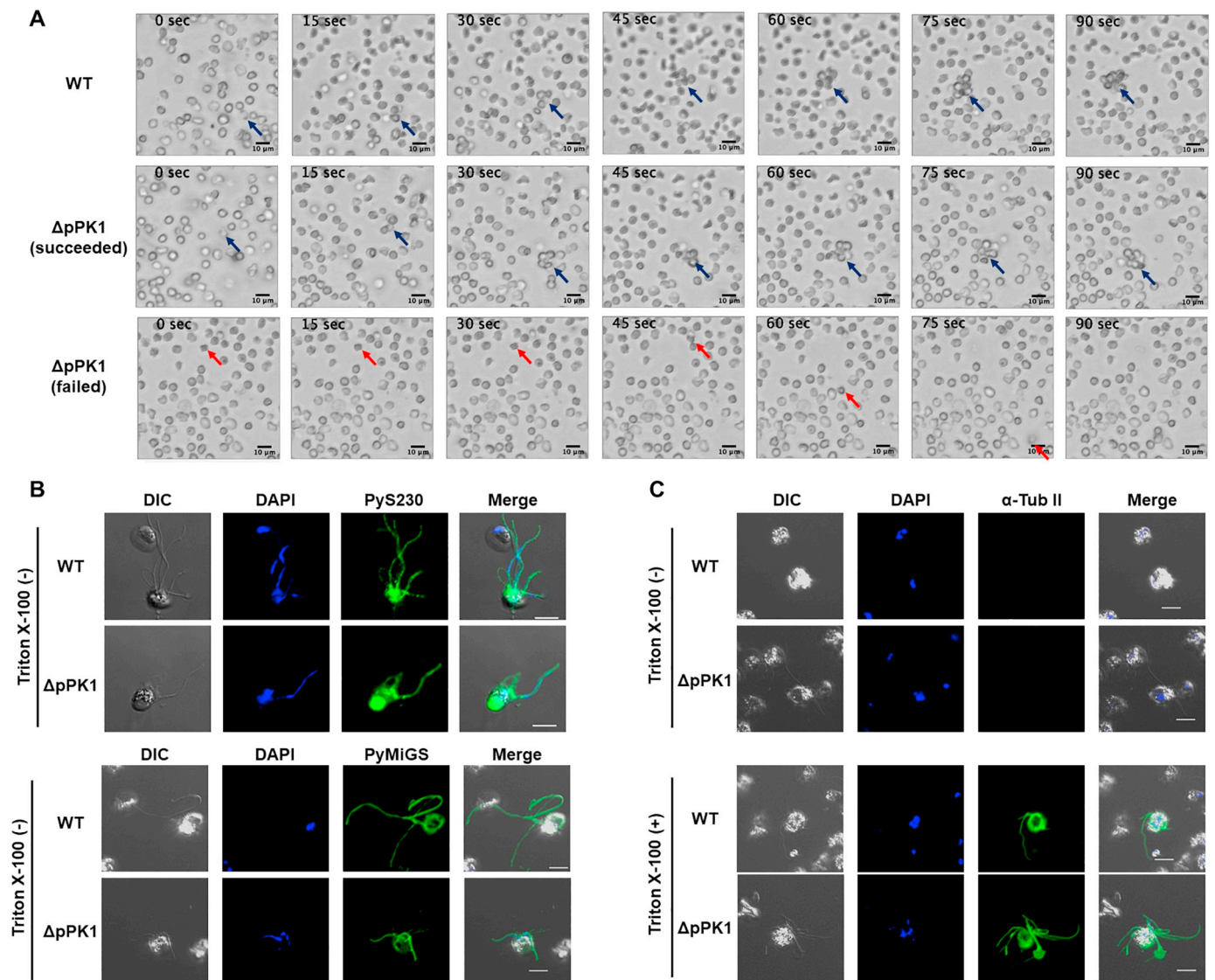


Fig. 7. PyS230 and PyMiGS were detected on the microgamete surface of Δ pPK1 parasites. (A) Representative images of exflagellated male gametocytes from time lapse imaging. Wild type (WT), Δ pPK1 #1 showing an exflagellation center, and Δ pPK1 #1 that failed to form a center are shown. Time stamp 0 s indicates the time point at 5 min after XA induction. Images were captured every 15 s from 0 to 90 s. Blue and red arrows indicate exflagellated male gametocytes. (B) IFA images of non-permeabilized microgametes of WT and Δ pPK1 #1 parasites reacted with anti-PyS230 antibody (top) and with anti-PyMiGS antibodies (bottom). (C) IFA images of non-permeabilized (top) or permeabilized (bottom) microgametes of WT and Δ pPK1 #1 parasites reacted with anti- α -tubulin II antibody (α -Tub II). Nuclei were stained with DAPI (blue). Scale bar 5 μ m. (For interpretation of the references to colour in this figure legend, the reader is referred to the web version of this article.)

1.0–13.5) (Fig. 6F), consistent with the decreased number of exflagellation center formation.

3.5. Deletion of pPK1 did not affect the microgamete surface localization of PyS230 and PyMiGS

Eksi et al. (2006) reported that disruption of the microgamete surface protein Pfs230, a soluble protein with an N-terminal signal peptide sequence and an array of 6-cysteine motif domains, in *P. falciparum* resulted in a significant reduction in exflagellation center formation [42], a phenotype similar to our observation for the *P. yoelii* Δ pPK1 parasites. *P. yoelii* microgamete surface protein (PyMiGS) is a protein with an N-terminal signal peptide sequence, aspartyl protease-like domain, and one transmembrane region at the C-terminal side and is expressed within the osmiophilic body of male gametocytes and on the microgamete surface [31]. The deletion mutant of PyMiGS in *P. yoelii* showed an impaired exflagellation activity [31]. Thus, we examined whether the microgamete surface localization of PyS230, a *P. yoelii* ortholog of Pfs230, and

PyMiGS is affected in Δ pPK1 parasites. IFA against microgametes under non-permeabilized condition was able to detect PyS230 and PyMiGS on the surface of Δ pPK1 microgametes similar to wild type parasites (Fig. 7B), indicating that pPK1 did not affect the surface localization of PyS230 and PyMiGS. Antibody against a cytoplasmic protein α -tubulin II did not stain microgametes under non-reducing conditions, confirming that the plasma membrane was intact (Fig. 7C).

4. Discussion

In this study we analyzed a *Plasmodium yoelii* pseudokinase (PypPK1; PY17X_1220300) that is highly expressed in both schizont and male gametocyte stages of *P. berghei*. Deletion of PypPK1 resulted in a significant growth defect and lower erythrocyte invasion efficacy compared to the parental parasite line. Although no differences were seen in male and female gametocytemias and gametocyte egress rates, the number of exflagellation centers and midgut oocysts were significantly reduced in the PypPK1 deletion mutant lines.

We showed that PypPK1 participates in regulation of parasite erythrocyte invasion. During this process, merozoites sequentially secrete microorganellar proteins such as AMA1 from micronemes and EBL from dense granules, in the case of the *P. yoelii* 17XL line [29,40]. AMA1 secretion is regulated by a hierarchical phosphorylation cascade by PKAc (cAMP-dependent protein kinase catalytic subunit) and GSK3 (glycogen synthase kinase 3) [43,44]. Thus we thought that PypPK1 could be involved in the process to discharge these microorganelles. Indeed, Flueck et al. (2019) recently reported that when PDE β , a molecule responsible for cAMP regulation and located upstream of PKA in the same signal cascade, was conditionally disrupted in *P. falciparum*, the pPK1 ortholog was phosphorylated > 2-fold relative to the control [45]. This suggested possible involvement of pPK1 in a cAMP signaling cascade. If this is the case, secretion of microorganellar proteins could be affected; however, we did not see clear differences for at least the secretion of AMA1 and EBL in the PypPK1-deleted *P. yoelii* 17XL line. Recent phosphor-proteome analysis of a *P. falciparum* line, in which the PKAc gene was conditionally disrupted, did not detect pPK1 as a substrate of PKA [46], which was not inconsistent to our result. Together, pPK1 appears to be involved in processes not linked to microorganellar discharge events.

PypPK1 signals were localized at the apical side of the merozoite and a punctate pattern was seen at the ookinete stage; however, they were colocalized with nuclei at the gametocyte and gamete stages, even though a nuclear localization sequence was not predicted [27]. Colocalization with nucleus signals were not seen at the merozoite and ookinete stages. Nucleus localization of pseudokinases without NLS have been reported in other organisms. For example, the pseudokinase Tra1 of *Saccharomyces cerevisiae* is a phosphatidylinositol 3-kinase-related kinase family protein without NLS but is transported to and anchored at the nucleus using its C-terminal phosphoinositide 3-kinase domain [47]. Another example is a vaccinia B12 pseudokinase, which interplays with B1 kinase and has a potent inhibitory activity [48]. PypPK1 signals overlapping with the nucleus at gametocyte and gamete stages may indicate that this protein is anchored and has a role at the nucleus at these stages.

This is the second report after Pfs230 to exhibit a phenotype of reduced exflagellation center formation in malaria parasites, without reducing the number of exflagellated male gametocytes. Aberrant morphology and motility were not clearly observable for Δ PypPK1 male gametocytes (Movie S2, S3), thus this is due to the reduced adherence activity of the microgametes to erythrocytes (Movie S3). Templeton et al. (1998) showed that human erythrocyte adherence to *P. falciparum* microgametes is sialic acid and glycophorin A dependent and that infectivity to mosquitoes is significantly reduced when sialic acids are removed from gametocyte-infected human erythrocytes [49]. Thus, we interpreted that the reduction of exflagellation formation observed in Δ PypPK1 parasite lines participated in the reduced oocyst numbers. However, because we did not assess the effect of Δ PypPK1 on steps after exflagellation center formation and before oocyst formation, other steps could also participate in the reduced oocyst numbers. The reduced activity of microgametes to adhere to erythrocytes could be due to the surface exposure of parasite adhesins; however, this is unlikely the case because we found two such candidate proteins PyS230 and PyMiGS were detected on the surface of the microgametes of Δ pPK1 parasites. Thus at least pPK1 is not responsible for the surface localization of these proteins. If they are responsible for erythrocyte adherence, their function may be affected in Δ PypPK1; for example, through altered post-translational modification or complex formation with other molecules.

In conclusion, we characterized a novel pseudokinase pPK1 in *P. yoelii* and showed that it possesses roles in merozoite invasion and exflagellation center formation. Further studies to determine the mode of action of this and other pseudokinases are of paramount interest and would provide potential targets to fight against malaria.

Supplementary data to this article can be found online at <https://doi.org/10.1016/j.parint.2020.102056>.

Acknowledgements

We thank Dr. Soldati-Favre D, and the Wellcome genome campus advanced course for the plasmid and Dr. Culleton R for mosquitoes. This study was performed at the Joint Usage/Research Center on Tropical Disease, Institute of Tropical Medicine (NEKKEN), Nagasaki University, Japan. TI is a recipient of the Japanese Society of Promotion Science (JSPS) DC1 scholarship. This study was supported in-part by JSPS KAKENHI grants (16H05184 and 19H03461 to OK and 17J09408 to TI). The funders have no role in this study design, data collection and analysis, decision to publish, or preparation of the manuscript.

Declaration of Competing Interest

None.

References

- [1] World Health Organization, World Malaria Report 2018, World Health Organization, (2018) Geneva, Switzerland.
- [2] M. De Niz, E. Meibalan, P. Mejia, S. Ma, N.M.B. Brancucci, C. Agop-Nersesian, R. Mandt, P. Ngotho, K.R. Hughes, A.P. Waters, C. Huttenhower, J.R. Mitchell, R. Martinelli, F. Frischknecht, K.B. Seydel, T. Taylor, D. Milner, V.T. Heussler, M. Marti, *Plasmodium* gametocytes display homing and vascular transmigration in the host bone marrow, *Sci. Adv.* 4 (2018) 1–15, <https://doi.org/10.1126/sciadv.aat3775>.
- [3] K.K. Ojo, C. Pfander, N.R. Mueller, C. Burstroem, E.T. Larson, C.M. Bryan, A.M.W. Fox, M.C. Reid, S.M. Johnson, R.C. Murphy, M. Kennedy, H. Mann, D.J. Leibly, S.N. Hewitt, C.L. Verlinde, S. Kappe, E.A. Merritt, D.J. Maly, O. Billker, W.C. Van Voorhis, Transmission of malaria to mosquitoes blocked by bumped kinase inhibitors, *J. Clin. Invest.* 122 (2012) 2301–2305, <https://doi.org/10.1172/JCI61822>.
- [4] M. Ganter, J.M. Goldberg, J.D. Dvorin, J.A. Paulo, J.G. King, A.K. Tripathi, A.S. Paul, J. Yang, I. Coppens, R.H.Y. Jiang, B. Elsworth, D.A. Baker, R.R. Dinglasan, S.P. Gygi, M.T. Duraisingh, *Plasmodium falciparum* CRK4 directs continuous rounds of DNA replication during schizogony, *Nat. Microbiol.* 2 (2017) 17017, <https://doi.org/10.1038/nmicrobiol.2017.17>.
- [5] B.M. Invergo, M. Brochet, L. Yu, J. Choudhary, P. Beltrao, O. Billker, Sub-minute phosphoregulation of cell cycle systems during *Plasmodium* gamete formation, *Cell Rep.* 21 (7) (2017) 2017–2029, <https://doi.org/10.1016/j.celrep.2017.10.071>.
- [6] E. Lasonder, J.L. Green, G. Camarda, H. Talabani, A.A. Holder, G. Langsley, P. Alano, *The Plasmodium falciparum* schizont phosphoproteome reveals extensive phosphatidylinositol and cAMP-protein kinase signaling, *J. Proteome Res.* 11 (11) (2012) 5323–5337, <https://doi.org/10.1021/pr300557m>.
- [7] A. Bansal, A. Molina-Cruz, L. Brzostowski, J. Mu, L.H. Miller, *Plasmodium falciparum* calcium-dependent protein kinase 2 is critical for male gametocyte exflagellation but not essential for asexual proliferation, *mBio* 8 (5) (2017) 1–17, <https://doi.org/10.1128/mbio.01656-17>.
- [8] A. Bansal, A. Molina-Cruz, J. Brzostowski, P. Liu, Y. Luo, K. Gunalan, Y. Li, J.M.C. Ribeiro, L.H. Miller, PfCDPK1 is critical for malaria parasite gametogenesis and mosquito infection, *Proc. Natl. Acad. Sci. U. S. A.* 115 (4) (2018) 774–779, <https://doi.org/10.1073/pnas.1715443115>.
- [9] O. Billker, S. Dechamps, R. Tewari, G. Wenig, B. Franke-Fayard, V. Brinkmann, Calcium and a calcium-dependent protein kinase regulate gamete formation and mosquito transmission in a malaria parasite, *Cell* 117 (4) (2004) 503–514, [https://doi.org/10.1016/s0092-8674\(04\)00449-0](https://doi.org/10.1016/s0092-8674(04)00449-0).
- [10] D. Dorin, K. Le Roch, P. Sallicandro, P. Alano, D. Parzy, P. Pouillet, L. Meijer, C. Doerig, Pfnk-1, a NIMA-related kinase from the human malaria parasite *Plasmodium falciparum*, *Eur. J. Biochem.* 268 (9) (2001) 2600–2608, <https://doi.org/10.1046/j.1432-1327.2001.02151.x>.
- [11] Y.M. Lye, M. Chan, T.S. Sim, Pfnk3: an atypical activator of a MAP kinase in *Plasmodium falciparum*, *FEBS Lett.* 580 (26) (2006) 6083–6092, <https://doi.org/10.1016/j.febslet.2006.10.003>.
- [12] R. Rangarajan, A.K. Bei, D. Jethwaney, P. Maldonado, D. Dorin, A.A. Sultan, C. Doerig, A mitogen-activated protein kinase regulates male gametogenesis and transmission of the malaria parasite *Plasmodium berghei*, *EMBO Rep.* 6 (5) (2005) 464–469, <https://doi.org/10.1038/sj.embo.7400404>.
- [13] R. Tewari, U. Straschil, A. Bateman, U. Böhme, I. Cherevach, P. Gong, A. Pain, O. Billker, The systematic functional analysis of *Plasmodium* protein kinases identifies essential regulators of mosquito transmission, *Cell Host Microbe* 8 (4) (2010) 377–387, <https://doi.org/10.1016/j.chom.2010.09.006>.
- [14] V. Reiterer, P.A. Eyers, H. Farhan, Day of the dead: pseudokinases and pseudo-phosphatases in physiology and disease, *Trends Cell Biol.* 24 (9) (2014) 489–505, <https://doi.org/10.1016/j.tcb.2014.03.008>.
- [15] K.R. Buchholz, P.W. Bowyer, J.C. Boothroyd, Bradyzoite pseudokinase 1 is crucial for efficient oral infectivity of the *Toxoplasma gondii* tissue cyst, *Eukaryot. Cell* 12 (3) (2013) 399–410, <https://doi.org/10.1128/EC.00343-12>.
- [16] R.D. Etheridge, A. Alaganan, K. Tang, H.J. Lou, B.E. Turk, L.D. Sibley, The *Toxoplasma* pseudokinase ROP5 forms complexes with ROP18 and ROP17 kinases that synergize to control acute virulence in mice, *Cell Host Microbe* 15 (5) (2014)

- 537–550, <https://doi.org/10.1016/j.chom.2014.04.002>.
- [17] M.L. Reese, N. Shah, J.C. Boothroyd, The *Toxoplasma* pseudokinase ROP5 is an allosteric inhibitor of the immunity-related GTPases, *J. Biol. Chem.* 289 (40) (2014) 27849–27858, <https://doi.org/10.1074/jbc.M114.567057>.
- [18] P. Ward, L. Equinet, J. Packer, C. Doerig, Protein kinases of the human malaria parasite *Plasmodium falciparum*: the kinome of a divergent eukaryote, *BMC Genomics* 5 (2004) 1–19, <https://doi.org/10.1186/1471-2164-5-79>.
- [19] B. Gnangnon, A. Fréville, C. Caillaud, C. Leroy, C. De Witte, D. Tulasne, A. Martoriarti, V. Jung, I.C. Guerrero, S. Marion, J. Khalife, C. Pierrot, *Plasmodium* pseudo-tyrosine kinase-like binds PP1 and SERA5 and is exported to host erythrocytes, *Sci. Rep.* 9 (1) (2019) 1–21, <https://doi.org/10.1038/s41598-019-44542-3>.
- [20] E. Bushnell, A.R. Gomes, T. Sanderson, B. Anar, G. Girling, C. Herd, T. Metcalf, K. Modrzynska, F. Schwach, R.E. Martin, M.W. Mather, G.I. McFadden, L. Parts, G.G. Rutledge, A.B. Vaidya, K. Wengelnik, J.C. Rayner, O. Billker, Functional profiling of a *Plasmodium* genome reveals an abundance of essential genes, *Cell* 170 (2) (2017) 260–272.e8, <https://doi.org/10.1016/j.cell.2017.06.030>.
- [21] M. Zhang, C. Wang, T.D. Otto, J. Oberstaller, X. Liao, S.R. Adapa, K. Udenze, I.F. Bronner, D. Casandra, M. Mayho, J. Brown, S. Li, J. Swanson, J.C. Rayner, R.H.Y. Jiang, J.H. Adams, Uncovering the essential genes of the human malaria parasite *Plasmodium falciparum* by saturation mutagenesis, *Science* 360 (6388) (2018) eaap7847, <https://doi.org/10.1126/science.aap7847>.
- [22] A.R. Gomes, E. Bushnell, F. Schwach, G. Girling, B. Anar, M.A. Quail, C. Herd, C. Pfander, K. Modrzynska, J.C. Rayner, O. Billker, A genome-scale vector resource enables high-throughput reverse genetic screening in a malaria parasite, *Cell Host Microbe* 17 (3) (2015) 404–413, <https://doi.org/10.1016/j.chom.2015.01.014>.
- [23] C. Aurécochea, J. Brestelli, B.P. Brunk, J. Dommer, S. Fischer, B. Gajria, X. Gao, A. Gingle, G. Grant, O.S. Harb, M. Heiges, F. Innamorato, J. Iodice, J.C. Kissinger, E. Kraemer, W. Li, J.A. Miller, V. Nayak, C. Pennington, D.F. Pinney, D.S. Roos, C. Ross, C. Stoeckert C.J. Jr, H. Wang Treatman, PlasmoDB: a functional genomic database for malaria parasites, *Nucleic Acids Res.* 37 (Database) (2009) D539–D543, <https://doi.org/10.1093/nar/gkn814>.
- [24] K. Katoh, K. Misawa, K. Kuma, T. Miyata, MAFFT: a novel method for rapid multiple sequence alignment based on fast Fourier transform, *Nucleic Acids Res.* 30 (14) (2002) 3059–3066, <https://doi.org/10.1093/nar/gkf436>.
- [25] J.J. Almagro Armenteros, K.D. Tsirigos, C.K. Sønderby, T.N. Petersen, O. Winther, S. Brunak, G. von Heijne, H. Nielsen, SignalP 5.0 improves signal peptide predictions using deep neural networks, *Nat. Biotechnol.* 37 (4) (2019) 420–423, <https://doi.org/10.1038/s41587-019-0036-z>.
- [26] A. Krogh, B. Larsson, G. von Heijne, E.L. Sonnhammer, Predicting transmembrane protein topology with a hidden Markov model: application to complete genomes, *J. Mol. Biol.* 305 (3) (2001) 567–580, <https://doi.org/10.1006/jmbi.2000.4315>.
- [27] J.R. Lin, J. Hu, SeqNLS: nuclear localization signal prediction based on frequent pattern mining and linear motif scoring, *PLoS One* 8 (10) (2013) e76864, <https://doi.org/10.1371/journal.pone.0076864>.
- [28] M.Y.X. Lim, G. LaMonte, M.C.S. Lee, C. Reimer, B.H. Tan, V. Corey, B.F. Tjahjadi, A. Chua, M. Nachon, R. Wintjens, P. Gedeck, B. Malleret, L. Renia, G.M.C. Bonamy, P.C.L. Ho, B.K.S. Yeung, E.D. Chow, L. Lim, D.A. Fidock, T.T. Diagana, E.A. Winzeler, P. Bifani, UDP-galactose and acetyl-CoA transporters as *Plasmodium* multidrug resistance genes, *Nat. Microbiol.* 1 (2016) 16166, <https://doi.org/10.1038/nmicrobiol.2016.166>.
- [29] Y. Kegawa, M. Asada, T. Ishizaki, K. Yahata, O. Kaneko, Critical role of erythrocyte binding-like protein of the rodent malaria parasite *Plasmodium yoelii* to establish an irreversible connection with the erythrocyte during invasion, *Parasitol. Int.* 67 (6) (2018) 706–714, <https://doi.org/10.1016/j.parint.2018.07.006>.
- [30] M.C.S. Lee, S.E. Lindner, J.J. Lopez-Rubio, M. Llinás, Cutting back malaria: CRISPR/Cas9 genome editing of *Plasmodium*, *Brief Funct. Genomics* 18 (5) (2019) 281–289, <https://doi.org/10.1093/bfgp/ezl021>.
- [31] M. Tachibana, T. Ishino, E. Takashima, T. Tsuboi, M. Torii, A male gametocyte osmiophilic body and microgamete surface protein of the rodent malaria parasite *Plasmodium yoelii* (PyMiGS) plays a critical role in male osmiophilic body formation and exflagellation, *Cell. Microbiol.* 20 (5) (2018) 1–12, <https://doi.org/10.1111/cmi.12821>.
- [32] N. Shinzawa, T. Ishino, M. Tachibana, T. Tsuboi, M. Torii, Phenotypic dissection of a *Plasmodium*-refractory strain of malaria vector *Anopheles stephensi*: the reduced susceptibility to *P. berghei* and *P. yoelii*, *PLoS One* 8 (5) (2013) e63753, <https://doi.org/10.1371/journal.pone.0063753>.
- [33] J.K. Mutungi, K. Yahata, M. Sakaguchi, O. Kaneko, Expression and localization of rhothry neck protein 5 in merozoites and sporozoites of *Plasmodium yoelii*, *Parasitol. Int.* 63 (6) (2014) 794–801, <https://doi.org/10.1016/j.parint.2014.07.013>.
- [34] H. Otsuki, O. Kaneko, A. Thongkukiatkul, M. Tachibana, H. Iriko, S. Takeo, T. Tsuboi, M. Torii, Single amino acid substitution in *Plasmodium yoelii* erythrocyte ligand determines its localization and controls parasite virulence, *Proc. Natl. Acad. Sci. U. S. A.* 106 (17) (2009) 7167–7172, <https://doi.org/10.1073/pnas.0811313106>.
- [35] J.K. Mutungi, K. Yahata, M. Sakaguchi, O. Kaneko, Isolation of invasive *Plasmodium yoelii* merozoites with a long half-life to evaluate invasion dynamics and potential invasion inhibitors, *Mol. Biochem. Parasitol.* 204 (1) (2015) 26–33, <https://doi.org/10.1016/j.molbiopara.2015.12.003>.
- [36] J.A. Simpson, K. Silamut, K. Chotivanich, S. Pukrittayakane, N.J. White, Red cell selectivity in malaria: a study of multiple-infected erythrocytes, *Trans. R. Soc. Trop. Med. Hyg.* 93 (2) (1999) 165–168, [https://doi.org/10.1016/S0035-9203\(99\)90295-X](https://doi.org/10.1016/S0035-9203(99)90295-X).
- [37] K. Thawnashom, M. Kaneko, P. Xangsayarath, N. Chaiyawong, K. Yahata, M. Asada, J.H. Adams, O. Kaneko, Validation of *Plasmodium vivax* centromere and promoter activities using *Plasmodium yoelii*, *PLoS One* 14 (12) (2019) e0226884, <https://doi.org/10.1371/journal.pone.0226884>.
- [38] J. Schindelin, I. Arganda-Carreras, E. Frise, V. Kaynig, M. Longair, T. Pietzsch, S. Preibisch, C. Rueden, S. Saalfeld, B. Schmid, J.Y. Tinevez, D.J. White, V. Hartenstein, K. Eliceiri, P. Tomancak, A. Cardona, Fiji: an open-source platform for biological-image analysis, *Nat. Methods* 9 (7) (2012) 676–682, <https://doi.org/10.1038/nmeth.2019>.
- [39] A. Marchler-Bauer, S.H. Bryant, CD-search: protein domain annotations on the fly, *Nucleic Acids Res.* 32 (Web Server issue) (2004) W327–W331, <https://doi.org/10.1093/nar/gkh454>.
- [40] S. Singh, M.M. Alam, I. Pal-Bhowmick, J.A. Brzostowski, C.E. Chitnis, Distinct external signals trigger sequential release of apical organelles during erythrocyte invasion by malaria parasites, *PLoS Pathog.* 6 (2) (2010) e1000746, <https://doi.org/10.1371/journal.ppat.1000746>.
- [41] O. Billker, M.K. Shaw, I.W. Jones, S.V. Ley, A.J. Mordue, R.E. Sinden, Azadirachtin disrupts formation of organised microtubule arrays during microgametogenesis of *Plasmodium berghei*, *J. Eukaryot. Microbiol.* 49 (6) (2002) 489–497, <https://doi.org/10.1111/j.1550-7408.2002.tb00234.x>.
- [42] S. Eksi, B. Czesny, G.J. Van Gemert, R.W. Sauerwein, W. Eling, K.C. Williamson, Malaria transmission-blocking antigen, Pfs230, mediates human red blood cell binding to exflagellating male parasites and oocyst production, *Mol. Microbiol.* 61 (4) (2006) 991–998, <https://doi.org/10.1111/j.1365-2958.2006.05284.x>.
- [43] K. Leykauf, M. Treeck, P.R. Gilson, T. Nebl, T. Braulke, A.F. Cowman, T.W. Gilberger, B.S. Crabb, Protein kinase a dependent phosphorylation of apical membrane antigen 1 plays an important role in erythrocyte invasion by the malaria parasite, *PLoS Pathog.* 6 (6) (2010) e1000941, <https://doi.org/10.1371/journal.ppat.1000941>.
- [44] B. Prinz, K.L. Harvey, L. Wilcke, U. Ruch, K. Engelberg, L. Biller, I. Lucet, S. Erkelenz, D. Heincke, T. Spielmann, C. Doerig, C. Kunick, B.S. Crabb, P.R. Gilson, T.W. Gilberger, Hierarchical phosphorylation of apical membrane antigen 1 is required for efficient red blood cell invasion by malaria parasites, *Sci. Rep.* 6 (2016) 34479, <https://doi.org/10.1038/srep34479>.
- [45] C. Flueck, L.G. Drought, A. Jones, A. Patel, A.J. Perrin, E.M. Walker, S.D. Nofal, A.P. Snijders, M.J. Blackman, D.A. Baker, Phosphodiesterase beta is the master regulator of cAMP signalling during malaria parasite invasion, *PLoS Biol.* 17 (2) (2019) e3000154, <https://doi.org/10.1371/journal.pbio.3000154>.
- [46] A. Patel, A.J. Perrin, H.R. Flynn, C. Bisson, C. Withers-Martinez, M. Treeck, C. Flueck, G. Nicastro, S.R. Martin, A. Ramos, T.W. Gilberger, A.P. Snijders, M.J. Blackman, D.A. Baker, Cyclic AMP signalling controls key components of malaria parasite host cell invasion machinery, *PLoS Biol.* 17 (5) (2019) e3000264, <https://doi.org/10.1371/journal.pbio.3000264>.
- [47] M.D. Berg, J. Genereaux, J. Karagiannis, C.J. Brandl, The pseudokinase domain of *Saccharomyces cerevisiae* Tra1 is required for nuclear localization and incorporation into the SAGA and NuA4 complexes, *G3 (Bethesda)* 8 (6) (2018) 1943–1957, <https://doi.org/10.1534/g3.118.200288>.
- [48] A.T. Olson, Z. Wang, A.B. Rico, M.S. Wiebe, A poxvirus pseudokinase represses viral DNA replication via a pathway antagonized by its paralog kinase, *PLoS Pathog.* 15 (2) (2019) e1007608, <https://doi.org/10.1371/journal.ppat.1007608>.
- [49] T.J. Templeton, D.B. Keister, O. Muratova, J.L. Procter, D.C. Kaslow, Adherence of erythrocytes during exflagellation of *Plasmodium falciparum* microgametes is dependent on erythrocyte surface sialic acid and glycoporphins, *J. Exp. Med.* 187 (10) (1998) 1599–1609, <https://doi.org/10.1084/jem.187.10.1599>.